JACS
JOURNAL OF THE AMERICAN CHEMICAL SOCIETY
Article
Cite This: J. Am. Chem. Soc. 2019, 141, 17180−17188
pubs.acs.org/JACS

Tracking the Metal-Centered Triplet in Photoinduced Spin Crossover of $Fe(phen)_3^{2+}$ with Tabletop Femtosecond M-Edge X-ray Absorption Near-Edge Structure Spectroscopy

Kaili Zhang,[†] Ryan Ash,[†] Gregory S. Girolami, and Josh Vura-Weis*

Department of Chemistry, University of Illinois at Urbana−Champaign, Urbana, Illinois 61801, United States

Supporting Information

ABSTRACT: Fe(II) coordination complexes are promising alternatives to Ru(II) and Ir(III) chromophores for photoredox chemistry and solar energy conversion, but rapid deactivation of the initial metal-to-ligand charge transfer (MLCT) state to low-lying (d,d) states limits their performance. Relaxation to a long-lived quintet state is postulated to occur via a metal-centered triplet state, but this mechanism remains controversial. We use femtosecond extreme ultraviolet (XUV) transient absorption spectroscopy to measure the excited-state relaxation of $Fe(phen)_3^{2+}$ and conclusively identify a ^3T intermediate that forms in 170 fs and decays to a vibrationally hot $^5T_{2g}$ state in 39 fs. A coherent vibrational wavepacket with a period of 249 fs and damping time of 0.63 ps is observed on the $^5T_{2g}$ surface, and the spectrum of this oscillation serves as a fingerprint for the Fe−N symmetric stretch. The results show that the shape of the $M_{2,3}$-edge X-ray absorption near-edge structure (XANES) spectrum is sensitive to the electronic structure of the metal center, and the high-spin sensitivity, fast time resolution, and tabletop convenience of XUV transient absorption make it a powerful tool for studying the complex photophysics of transition metal complexes.

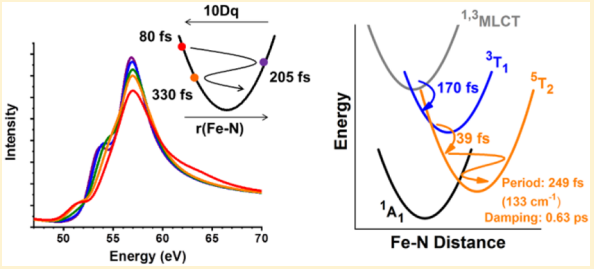

INTRODUCTION

In the past several years there has been a surge of interest in Fe^{II} polypyridyl complexes as chromophores for photocatalytic and photovoltaic applications, with the aim of replacing expensive Ru^{II} and Ir^{III} photosensitizers.[1−4] This goal is challenging because the weaker ligand field of first-row transition metals creates a cascade of low-lying metal-centered (MC) states that rapidly deactivate the initial excited state. For example, both $Ru(bpy)_3^{2+}$ (bpy = 2,2′-bipyridine) and $Fe(bpy)_3^{2+}$ have low-spin d^6 ground states and metal-to-ligand charge transfer (MLCT) states that lie 2−3 eV above the ground state. However, the MLCT state of $Ru(bpy)_3^{2+}$ has a lifetime of hundreds of nanoseconds whereas that of $Fe(bpy)_3^{2+}$ decays within 200 fs into a low-energy $^5T_{2g}$ state with 100% quantum yield.[5−7] Consequently, the energy is wasted as molecular vibrations long before any useful photochemistry can occur.

A typical potential energy surface and molecular orbital diagram for Fe^{II} polypyridyl complexes is given in Figure 1, showing metal-centered ^3T and $^5T_{2g}$ surfaces that cross the MLCT surface near its minimum. Chemists have tackled the challenge of rapid metal-centered deactivation by engineering molecules that either raise the energy of the MC states above the energy of the MLCT state (a thermodynamic solution) or displace/deform the excited-state potential energy surfaces of the MC states to trap molecules in high-energy metastable MLCT or triplet MC states (a kinetic solution).[3] These strategies have had some success: Fe^{II} complexes with excited-state lifetimes as long as 528 ps have been described.[8]

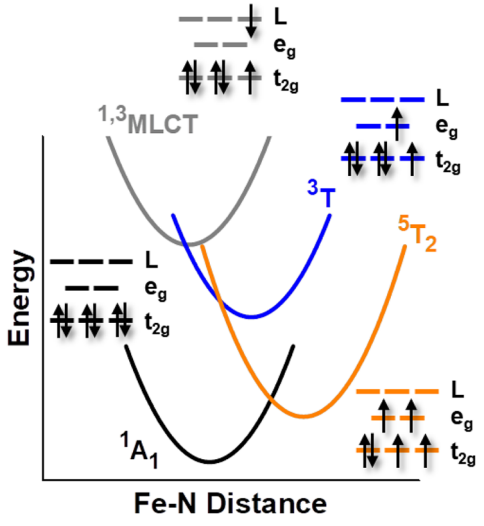

Figure 1. Potential energy surfaces and orbital occupations for common Fe^{II} polypyridyl complexes.

Despite these advances, there is still considerable uncertainty about the excited-state dynamics of Fe^{II} polypyridyl molecules, due to the complex interplay between electronic, spin, and nuclear degrees of freedom. Because a direct transition from

Received: July 10, 2019
Published: October 5, 2019

DOI: 10.1021/jacs.9b07332
J. Am. Chem. Soc. 2019, 141, 17180−17188

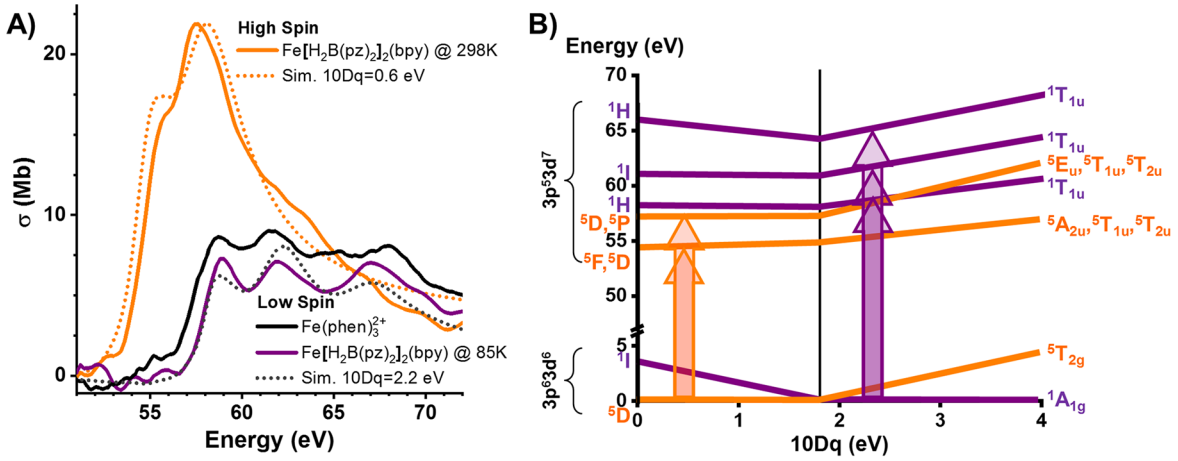

Figure 2. (A) Experimental and simulated $M_{2,3}$-edge spectra of high-spin and low-spin Fe^{II} complexes. (B) Correlation diagram showing the allowed XUV transitions between the $3p^63d^6$ ground state and the $3p^53d^7$ core-hole excited state as a function of the ligand field strength 10*Dq*. The break at 1.8 eV is caused by the crossover between a high-spin and low-spin ground state. The effects of spin−orbit coupling are weak and for simplicity are not shown.

^{1,3}MLCT to $^5T_{2g}$ involves the simultaneous movement of at least two electrons, it has long been suspected that conversion of the MLCT state to the $^5T_{2g}$ state occurs via a triplet metal-centered excited state ($^3T_{2g}$ or $^3T_{1g}$), but the role of this triplet remains controversial. Because the spin transition occurs in a region of the potential energy surface with curve crossings between multiple states, the formation of a triplet intermediate cannot be ruled out on theoretical grounds.[9,10] In addition, the formation of ^{3}T states cannot easily be probed by conventional visible-light transient absorption methods, because the d−d transitions are weak compared to the intense MLCT band. As a result, the spectra are relatively insensitive to the spin state of the metal center.

Other spectroscopic techniques have afforded conflicting information about whether triplet states are generated upon excitation of Fe^{II} polypyridyl complexes. The strongest evidence for the triplet intermediate comes from femtosecond Fe K_β X-ray emission spectroscopy (XES), which is sensitive to the spin state of the Fe center. In a series of reports,[11−13] Gaffney and co-workers compared the transient XES spectra of $Fe(bpy)_3^{2+}$ to ground-state spectra of a series of model complexes and showed that only a model that included a triplet intermediate state could fit the experimental results. By simultaneously measuring Fe K-edge XANES and X-ray diffuse scattering, they correlated the electronic changes with structural changes, highlighting the activation of the Fe−N symmetric stretch. However, Auböck and Chergui came to a different conclusion using femtosecond ultraviolet/visible transient absorption spectroscopy. Based on results using a UV probe sensitive to the quintet state and a visible probe sensitive to the MLCT state, they argued that a vibrationally hot quintet state is formed within 50 fs, which is too short to admit a triplet intermediate.[14]

Much of the success in designing new Fe^{II} chromophores derives from increased understanding of the excited-state potential energy surfaces and their crossing points, so it is crucial to resolve these differing proposals for the role of the ^{3}T intermediate. Intramolecular vibrational relaxation within each electronic state competes with intersystem crossing between states, so small changes in these surfaces, or in the initial photoexcitation conditions, may lead to large changes in the photophysics. A striking example of this fine-tuning was recently reported by Chábera et al. for the Fe^{II} carbene complex $Fe(btz)_3$, in which the excited-state dynamics depend sensitively on the excitation wavelength.[15] Although excitation of this molecule into high-energy MLCT bands at wavelengths shorter than 690 nm showed a competition between intramolecular vibrational relaxation (IVR) and intersystem crossing (ISC) to a ^{3}MC state, molecules excited into the lowest MLCT band at 825 nm lack sufficient vibrational energy to cross the barrier to the thermodynamically favorable ^{3}MC state. A similar strategy was employed to design an Fe^{III} carbene complex with a 2 ns ligand-to-metal charge transfer (LMCT) lifetime; again the system is kinetically trapped and unable to access a lower-energy MC state.[16]

In the present work, we use tabletop femtosecond extreme ultraviolet (XUV) transient absorption spectroscopy to provide direct and unambiguous evidence that a metal-centered triplet intermediate is generated following MLCT excitation of the Fe^{II} *o*-phenanthroline complex $Fe(phen)_3^{2+}$. We also find that a coherent vibrational wavepacket on the $^5T_{2g}$ surface leads to an oscillation in the transient spectrum that corresponds to the Fe−N symmetric stretch. Ligand field multiplet simulations confirm these assignments. These results illustrate the utility and power of X-ray absorption near edge structure (XANES) spectroscopy at the Fe $M_{2,3}$-edge, a technique that is sensitive to the oxidation state and spin state of the metal center as well as the ligand field symmetry and strength.[17−21]

EXPERIMENTAL SECTION

XUV Transient Absorption. The XUV probe is produced by high harmonic generation using a tabletop instrument described previously.[17,22] Briefly, a Ti:sapphire driving laser (800 nm, 4 mJ, 35 fs, 1 kHz) is focused into a semi-infinite gas cell filled with 120 Torr of neon, where the intense electric field at the focal point generates a ∼15 fs XUV pulse with a broad spectrum spanning 50−90 eV. Residual driving laser photons are attenuated by a Si mirror and a 100 nm thick Al filter. XUV photons are collected in transmission mode and dispersed by a diffraction grating onto an array charge-coupled device (CCD) detector. The spectrometer resolution is 0.6 eV full width at half maximum (fwhm) as measured from the atomic absorption lines of Xe. A secondary output from the driving laser is sent through a noncollinear optical parametric amplifier (TOPAS-

DOI: 10.1021/jacs.9b07332
J. Am. Chem. Soc. 2019, 141, 17180−17188

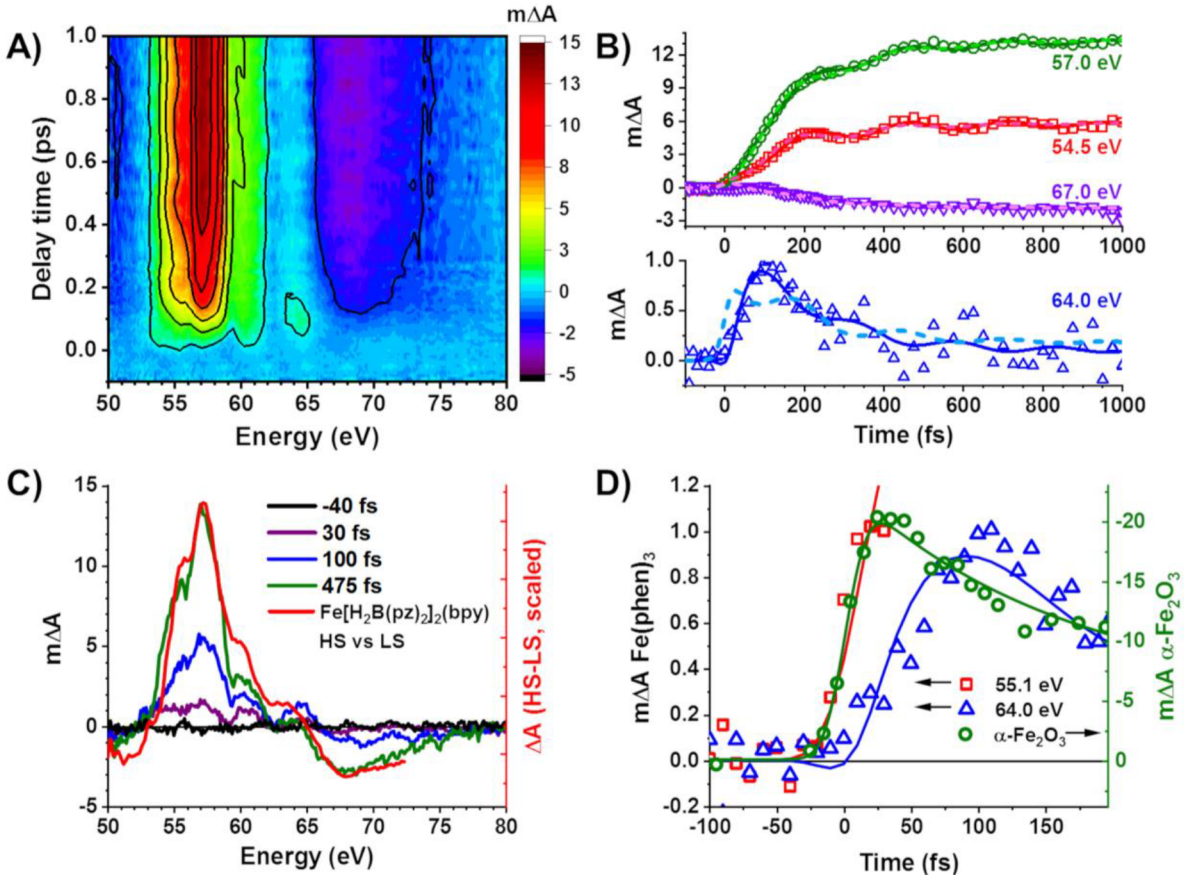

Figure 3. (A) Contour plot of transient M-edge XANES spectra of $Fe(phen)_3^{2+}$. (B) Experimental kinetic slices at selected energies (open symbols), with reconstructed kinetics from global fits. Solid lines include the ^3T intermediate, while dashed lines assume that the $^5T_2$ state is formed directly from the ^{1,3}MLCT state. The two fits are indistinguishable at 54.5, 57.0, and 67.0 eV, but only the ^{1,3}MLCT → ^3T → $^5T_{2g}$ model successfully fits the data at 64.0 eV. (C) Transient spectra of $Fe(phen)_3^{2+}$ at selected times, along with the thermal difference spectrum of $Fe[H_2B(pz)_2]_2(bpy)$ shown in red. (D) Experimental kinetic slices of $Fe(phen)_3^{2+}$ compared to the IRF-limited LMCT transition of α-Fe_2O_3, showing a an IRF-limited rise at 55.1 eV followed by the delayed rise of the feature at 64.0 eV. Fit lines for $Fe(phen)_3$ correspond to the three-state model described in the main text, and fit line for α-Fe_2O_3 is described in the Supporting Information.

White) to generate the pump pulse (35 fs, 535 nm). The instrument response function (IRF) is 40 fs fwhm, as determined by measuring the rise of α-Fe_2O_3 transient absorption features.[19,23] Samples were deposited as ~100 nm thick films on Si_3N_4 substrates. Further experimental details can be found in the Supporting Information.

Ligand-Field Multiplet Theory Simulations. The procedure for computing ligand field multiplet (LFM) theory simulations of $M_{2,3}$-edge spectra of metal-centered excited states using a modified version of the program CTM4XAS has been described in a previous publication.[20] Briefly, the metal center is modeled in terms of a parametric Hamiltonian containing electron−nuclear and electron−electron Coulombic interactions, spin−orbit coupling, and an electrostatic crystal field.[24,25] The parameters used in the present study can be found in the Supporting Information. The identities of the eigenstates of the Hamiltonian are assigned by expanding the spin−orbit coupled states in terms of pure-spin basis functions. $M_{2,3}$-edge stick spectra are computed between eigenstates of $3p^63d^N$ and $3p^53d^{N+1}$ configurations. Each transition is broadened by a Lorentzian whose width is determined by computing the Auger decay rate of the corresponding $3p^53d^{N+1}$ state. A floor of 1.0 eV is imposed to account for other decay channels. The transitions are further broadened by a Gaussian with σ = 0.2 eV to account for finite instrumental resolution.

The simulated spectrum of the $^1A_{1g}$ state of Fe^{II} has been rescaled to 60% of the computed intensity in accordance with the experimentally observed intensity difference in the spectra of the $^1A_{1g}$ and $^5T_{2g}$ states of $Fe[H_2B(pz)_2]_2(bpy)$. Simulated difference spectra of Fe^{II} metal-centered excited states are computed by subtracting the simulated absorption spectrum of the $^1A_{1g}$ state from those of the excited states. The difference spectrum of the MLCT excited state is computed as the difference of the simulated spectrum of the $^2T_{2g}$ state of Fe^{III} (rescaled to 60%) minus that of the $^1A_{1g}$ state of Fe^{II}. All spectra are shifted along the energy axis to place the degeneracy-weighted average transition energy at 56.4 eV for the $^1A_{1g}$ state, at 55.2 eV for all Fe^{II} metal-centered excited states, and at 56.2 eV for the Fe^{III} $^2T_{2g}$ state.

RESULTS AND DISCUSSION

Ground-State Spectra. XUV spectroscopy is performed using a tabletop laser-based source that produces a broad XUV continuum spanning the range from 50 to 90 eV (see Experimental Section). The ground-state spectrum of $Fe(phen)_3^{2+}$ is typical of low-spin Fe^{II} complexes[22] and features three peaks of approximately equal height at 58.7, 61.5, and 68.0 eV (Figure 2). To demonstrate the spin sensitivity of M-edge XANES and to estimate the transient spectrum upon spin crossover, we recorded the temperature-dependent ground-state spectra of the thermal spin crossover complex $Fe[H_2B(pz)_2]_2(bpy)$.[26] This model complex switches from a low-spin singlet to a high-spin (HS) quintet at 150 K. As shown in Figure 2A, the low-spin (LS) spectrum recorded at 85 K is similar to that of $Fe(phen)_3^{2+}$, with only minimal shifts in the peak positions. The HS spectrum recorded at room temper-

DOI: 10.1021/jacs.9b07332
J. Am. Chem. Soc. 2019, 141, 17180−17188

ature is red-shifted and ~3 times as intense, with a major peak at 57.5 eV and a shoulder at 55.6 eV. As is commonly observed in L-edge spectroscopy (2p → 3d excitation), HS spectra are generally red-shifted from their LS analogues due to additional exchange stabilization of the HS core-hole state.[27]

These spectra can be understood with the aid of the correlation diagram in Figure 2B, which is analogous to the Tanabe–Sugano diagrams used to interpret d–d excitations. The XUV probe measures transitions between the $3p^63d^6$ ground state and $3p^53d^7$ core-hole excited states. On the high-spin, weak-field (left) side of this diagram, transitions are allowed from the ^{5}D-derived ground state to a closely spaced group of ^{5}F- and ^{5}D-derived states at ~54 eV and another group of ^{5}D- and ^{5}P-derived states at ~57 eV. On the low-spin, strong-field (right) side of the diagram, the electronic state is better described by Mulliken term symbols within octahedral symmetry. Transitions are allowed between the $^1A_{1g}$ ground state and three $^1T_{1u}$ core-hole states; the transitions appear at approximately 58, 62, and 65 eV. The position of each peak depends on the ligand field splitting $10Dq$, making the spectrum a sensitive probe of the ligand field strength. Spin–orbit coupling is included in the actual spectral simulations but is weak enough to be omitted in this qualitative description.

Transient M-edge XANES and Kinetic Modeling. The femtosecond dynamics of $Fe(phen)_3^{2+}$ were measured by photoexciting the sample at its MLCT band with a 35 fs, 535 nm pump and probing with a 15 fs broadband XUV probe (see Experimental Section for a detailed description of the instrument). Figure 3A shows a contour plot of the transient absorption spectrum, where $\Delta A = -\log_{10}(I_{\text{pump on}}/I_{\text{pump off}})$. Spectroscopic slices at selected delay times are shown in Figure 3C. The IRF-limited initial state (as shown by the 30 fs slice) has a weak, broad positive feature between 53 and 62 eV. By 100 fs, a peak rises at 57.0 eV along with a shoulder at 61.0 eV and a small isolated peak at 64.0 eV. Over the next ~400 fs the peak at 57.0 eV rises further and develops a clear shoulder at 54.5 eV, and the peak at 64.0 eV disappears. A broad bleach from 65 to 75 eV also appears on this time scale. At times longer than 500 fs, the shape of the difference spectrum closely resembles the high-spin/low-spin thermal difference spectrum ($A_{\text{hot}} - A_{\text{cold}}$) of the iron(II) complex $Fe[H_2B(pz)_2]_2(bpy)$. This similarity confirms that photoexcitated $Fe(phen)_3^{2+}$ converts into a long-lived, high-spin state.

Kinetic slices at select energies are shown in Figure 3B, with the data shown as open symbols. Fits with and without the ^{3}T intermediate (discussed below) are shown as solid and dashed lines, respectively. Both the 57.0 eV peak and the 54.5 eV shoulder show clear oscillations with a period of ~250 fs. The relative amplitude of the oscillation is strongest at 54.5 eV, where it is 25% of the average signal. The peak at 64.0 eV rises to a maximum at 90 fs before decaying to near baseline by 400 fs. This rise is considerably delayed compared to the 40 fs fwhm instrumental response function, indicating that this signal is not due to the directly pumped ^{1}MLCT state or the rapidly formed ^{3}MLCT state.[28] The M-edge XANES spectrum is not sensitive to ferro/antiferromagnetic coupling between the metal and ligand spins, so the singlet and triplet MLCT states are expected to have identical spectra in this energy range. The delayed rise at 64.0 eV can be clearly seen in Figure 3D, where the IRF-limited bleach of α-Fe_2O_3 is compared to two slices at 55.1 and 64.0 eV. The 55.1 eV signal (assigned below to the MLCT state) rises with the IRF, whereas the 64.0 eV signal (assigned below to the metal-centered triplet) is delayed by ~40 fs.

Two different kinetic models were used to perform global fits of the transient M-edge XANES spectra of $Fe(phen)_3^{2+}$ versus time: (1) a three-state kinetic model that includes an intermediate (presumably ^{3}T) state, i.e., $^{1,3}\text{MLCT} \xrightarrow{\tau_1} {}^3\text{T} \xrightarrow{\tau_2} {}^5T_{2g}$ and (2) a two-state kinetic model that excludes this intermediate state, i.e., $^{1,3}\text{MLCT} \xrightarrow{\tau_1} {}^5T_{2g}$. In both models, the final $^5T_{2g}$ state has an additional damped oscillatory component. The process of spin crossover accompanied by vibrational coherence is modeled in terms of a spin-boson model in which the transitions between electronic states are treated phenomenologically as first-order processes.[10,29] Time zero was determined from concurrently measured transient absorption spectra of α-Fe_2O_3, which exhibits an IRF-limited population of a ligand-to-metal charge transfer (LMCT) state.[19] Additional details about the models used here, including explicit expressions of the modeled signal as a function of time, energy, and fit parameters, are included in the Supporting Information.

Fitting to the three-state model gives decay lifetimes of τ_1 = 170 ± 9 fs for the ^{1,3}MLCT state and τ_2 = 39 ± 6 fs for the ^{3}T intermediate (see Supporting Information for a description of the error estimation). The MLCT lifetime matches well with the range of reported lifetimes for MLCT states of related systems,[13,27,30−32] and τ_2 is in reasonable agreement with the value determined for $Fe(bpy)_3^{2+}$ by Fe K_β-edge emission (70 ± 30 fs).[13]

The period of oscillation of the final $^5T_{2g}$ state is 249 ± 9 fs, corresponding to a frequency of 133 ± 4 cm^{-1}. This frequency is ~15% higher than that of the 116 cm^{-1} fully symmetric breathing mode of HS $Fe(phen)_3^{2+}$ predicted by density functional theory (DFT) calculations (see Supporting Information for computational details). A difference of a similar magnitude between the observed coherent oscillation frequency and DFT-predicted vibrational frequency has been reported for crystalline $Fe(phen)_2(NCS)_2$ (expt. 116 vs DFT 96 cm^{-1}).[33,34] In both cases, the discrepancies between the computed and experimental frequencies are probably due to solid-state packing effects. As shown in the Supporting Information, a Fourier transform of the data reveals oscillatory features at ~55 and ~57 eV with a period of 123 cm^{-1}, consistent with the global fit.

The vibrational coherence of the final $^5T_{2g}$ state has a damping time of 0.63 ± 0.33 ps. The damping rate of vibrational coherence in condensed phases is highly variable. Our value, measured from an amorphous/nanocrystalline sample, falls within the range previously measured from solution samples (e.g., 0.4–1 ps depending on wavelength),[14,30] liquid jet samples (0.32 ps),[32] and crystalline solid samples (0.166 ps)[34] of related compounds. The time-dependent state populations and spectroscopic components obtained from this three-state fit are shown in Figure 4A and B. Reconstructed kinetic traces (Figure 3B) closely match the experimental results.

The two-state model without the ^{3}T intermediate fits the spectroscopic features at 54.5, 57.0, and 67.0 eV equally well, but the ^{3}T state is required to reproduce the 64.0 eV feature. For this reason, we will confine the rest of the present discussion to the three-state model with the ^{3}T intermediate. A detailed discussion of the two-state model is given in the

DOI: 10.1021/jacs.9b07332
J. Am. Chem. Soc. 2019, 141, 17180–17188

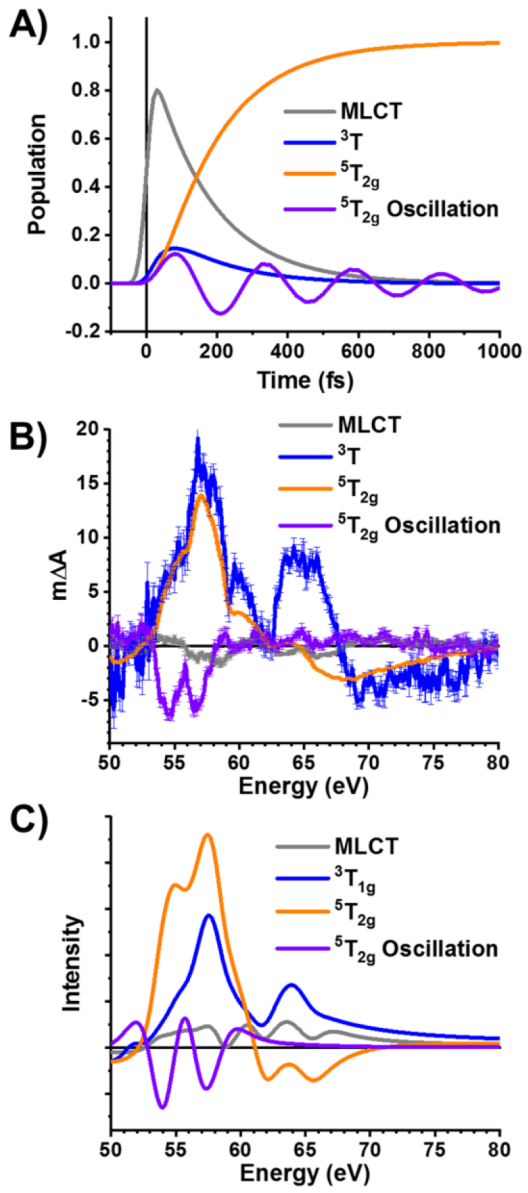

Figure 4. (A) Population of each species and amplitude of the oscillatory component of the $^5T_{2g}$ spectrum as a function of time. (B) Spectral components of the global fit to the ^{1,3}MLCT → ^{3}T → $^5T_{2g}$ model. Error bars on the spectra represent $\pm 1\sigma$ uncertainty of the fit. (C) Ligand field multiplet simulations of the transient spectra using the program CTM4XAS. The simulations are excellent qualitative matches for the experimental components in (B), in particular the 64 eV peak indicative of the ^{3}T intermediate.

Supporting Information, along with a comparison of the residual from each fit.

Additional information about the species formed upon photoexcitation of $Fe(phen)_3^{2+}$ is provided by the shapes of the spectral components deduced from the fit to the three-state model. As shown in Figure 4B, the spectrum of the MLCT state is quite weak, featuring a slight positive feature between 51 and 55 eV and a slight negative feature between 55 and 60 eV. As discussed in the Supporting Information, the low intensity of this transient spectrum is explained by a coincidental similarity between the $^1A_{1g}$ ground state and Fe^{III} $^2T_{2g}$ MLCT spectra. The fit also shows that the ^{3}T component has an intense positive feature at 57.0 eV, a shoulder at 60.0 eV, and a strong positive peak between 63 and 67 eV. Finally, the spectrum of the $^5T_{2g}$ component matches the 475 fs spectrum shown in Figure 3C, and the oscillatory component has two negative peaks at 54.7 and 56.8 eV.

These experimental components match ligand field multiplet (LFM) simulations carried out with the program CTM4XAS (Figure 4C). The extracted $^5T_{2g}$ spectrum agrees well with the corresponding simulation, which contains strong positive features at 54.8 and 57.4 eV and a broad bleach from 61 to 70 eV. The $^3T_{1g}$ simulation has peaks at 57.6 and 63.9 eV, which agree almost exactly with the spectrum of the intermediate deduced from the fit to the three-state model. As shown in the Supporting Information, a simulation of the $^3T_{2g}$ transient spectrum is also a good match to experiment, so this experiment cannot confidently distinguish between the two triplet states. In either case, the experimental spectrum is more intense than what LFM simulations suggest. In view of the rapid excited-state dynamics, which especially in the case of the ^{3}T intermediate permit only a single passage through the transition state to $^5T_{2g}$, the first-order kinetic model used here will underestimate the population of the intermediate and overestimate its spectral contribution.[35] A recent XES study of the transient electronic states also found evidence for ballistic excited-state evolution and showed that the triplet dynamics were better modeled by a 58 fs residence time in the ^{3}T state than by exponential kinetics.[12]

As noted earlier, a vibrational coherence with a period of 249 fs is observed on the $^5T_{2g}$ surface. The spectrum of this oscillation serves as a fingerprint for the structural distortion activated by the spin crossover event. The most prominent structural difference between the Franck−Condon geometry and the relaxed $^5T_{2g}$ geometry is the fully symmetric expansion of the Fe−N cage, which in the computational framework used here is modeled as a decrease in the ligand field strength 10*Dq*. Oscillation on the quintet surface therefore modulates 10*Dq*, leading to characteristic changes in the XANES spectrum.

Figure 5A shows a quantitative correlation diagram and contour plot of the M-edge XANES spectrum for high-spin Fe^{II} as a function of 10*Dq*. Note that several additional weakly allowed states are shown that were omitted in the qualitative diagram in Figure 2B. As was noted in the description of the ground-state spectra above, in the weak-field limit the spectrum is characterized by transitions from the ^{5}D ground state to ^{5}D and ^{5}F states at ∼54 eV and to ^{5}D and ^{5}P states at ∼57 eV. As the ligand field increases, these atomic states branch into multiple strong-field states, which broadens the spectrum and decreases the intensity at those energies. Therefore, a vibrational wavepacket launched on the compressed side of the Fe−N potential surface (large 10*Dq*) will initially have low absorbances at 54 and 57 eV, and the signal at these energies will reach a maximum one-half-period later at the outer turning point. This prediction is confirmed by the negative amplitude of the fitted oscillatory component in Figure 4C, which is an excellent match for the simulated component in Figure 4D.

Note that the kinetic model used in the fit properly accounts for the phase of the vibrational wavepacket: for example, the portion of the $^5T_{2g}$ population that is launched at times *t* and (*t* + 125 fs) (Figure 5C inset) will correspond to opposite extremes of the oscillatory relaxation. As a result, their contributions to the difference spectrum will be out of phase

DOI: 10.1021/jacs.9b07332
J. Am. Chem. Soc. 2019, 141, 17180−17188

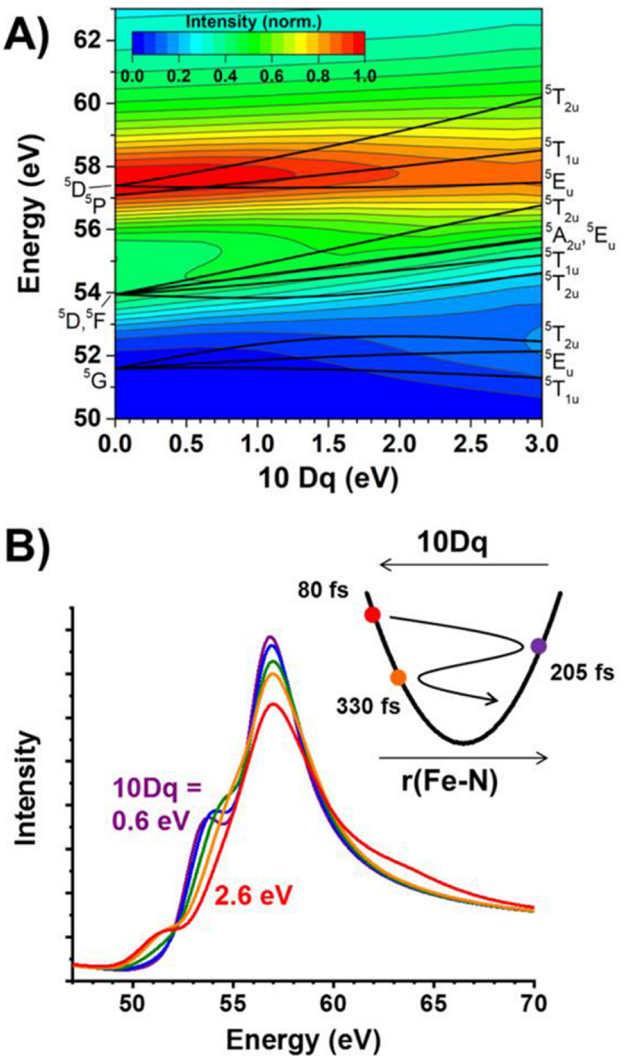

Figure 5. (A) Quantitative high-spin correlation diagram for 3p → 3d transitions in O_h Fe^{II} complexes as a function of the ligand field strength 10*Dq*, calculated from ligand field multiplet theory. The energies of allowed transitions are shown as the solid black lines, with the M-edge XANES spectrum shown as a heatmap. The lowest set of states (derived from the ^5G term) are forbidden in the weak-field limit and therefore have low oscillator strength until high 10*Dq*. (B) Spectra at selected values of 10*Dq*. As the ligand field strength increases and the atomic (weak-field) states branch into several strong-field states, the peaks at ∼54 and ∼57 eV broaden and lose intensity. The inset shows the coherent oscillation on the $^5T_{2g}$ potential energy surface and the inverse relationship between the Fe−N distance and 10*Dq*.

and be attenuated due to destructive interference. Figure 6 summarizes the full excited-state relaxation dynamics.

Comparison to Complementary Experiments. As noted in the Introduction, the strongest evidence for and against the triplet intermediate in iron(II) polypyridine complexes comes from transient XES and ultraviolet spectroscopy, respectively. In light of the present results, it is therefore useful to discuss the advantages and limitations of each technique. K_β emission spectroscopy, corresponding to 3p → 1s relaxation, is sensitive to the exchange interaction between the 3p and 3d electrons and therefore the spin state of the metal center.[36] The spectrum is relatively insensitive to the ligand field, and therefore, a transient spectrum can be

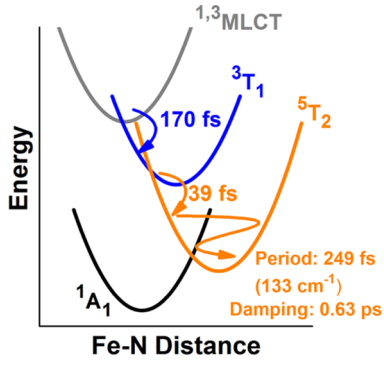

Figure 6. Summary of the excited-state relaxation observed for $Fe(phen)_3^{2+}$.

compared to the ground-state spectra of model complexes representing each possible spin state. By projecting the transient spectra onto these model-complex basis spectra, the population of each spin state can be estimated as a function of time after photoexcitation.

One possible drawback of XES studies is that, due to the relatively small instantaneous population of the metal-centered triplet state compared to that of the MLCT and quintet states, the projection is highly dependent on the choice of the model complex spectra. K_β spectra do show a small but measurable dependence on metal−ligand covalency, ligand field strength, and symmetry,[37,38] and it may not always be possible to identify model complexes whose spectra closely match those expected for the excited states of the sample under study. For example, a highly compressed quintet state could have a ligand field strength that is significantly higher than that of a chosen model complex.

A further potential complication with current femtosecond XES experiments is the high pump fluence used to collect transient spectra, in the range of 80−120 mJ/cm^2. Although these studies were careful to remain predominantly in the linear absorption regime, multiphoton absorption has the potential to perturb excited-state relaxation processes.[39,40] With the advent of free-electron lasers operating in the ∼1 MHz regime, however, transient XES experiments will soon be possible at lower excitation fluxes while maintaining high signal-to-noise.

A second technique, transient UV/visible spectroscopy, was used to probe both the MLCT state in the visible region and a signal at ∼310 nm that is characteristic of the metal-centered quintet. The high signal-to-noise ratio of this experiment enabled the observation of three distinct vibrational frequencies on the quintet surface even at the low pump fluence of ∼3 mJ/cm^2. A major challenge associated with studying the photoexcitation of iron(II) polypyridine complexes by UV/visible spectroscopy is the weak oscillator strengths of d−d transitions, so that the spin and oxidation state of the metal center must be inferred from the shape and position of charge-transfer transitions. An impediment in the analysis is the lack of good model complexes for the metal-centered triplet. In particular, the absorption spectrum of the ^3T state in the 300−320 nm region may be similar to that of the $^5T_{2g}$ state, at least while each state is vibrationally hot in the first tens of femtoseconds after spin crossover. The rise of the ∼310 nm peak observed in the transient UV experiment may therefore report on the combined population of ^3T and $^5T_{2g}$ states.

DOI: 10.1021/jacs.9b07332
J. Am. Chem. Soc. 2019, 141, 17180−17188

An advantage of M-edge XANES is that it combines the metal-specific nature of core-level spectroscopy with the in-lab convenience of laser-based sources. The strong 3p—3d overlap produces spectra with oscillator strengths on the same order as visible-light features. Strong transient signals are therefore observed at moderate pump fluences, 3.5 mJ/cm^2 in the present study, that are comparable to those in transient UV/visible spectroscopy. The strong angular momentum-dependent Coulomb and exchange interactions between the 3p core-hole and the 3d valence electrons lead to qualitatively distinct spectra for different spin states. These clear spectroscopic signatures make identification of intermediate states relatively straightforward. Furthermore, M-edge spectra are intuitive and can be described using traditional ligand field theory, and their sensitivity to ligand field strength and symmetry provides a fingerprint for specific normal modes in excited-state vibrational wavepackets.

Of course, this spectroscopic region also faces its own inherent challenges. One significant limitation of the XUV probe, which is not shared by visible and hard X-ray photons, is the short penetration depth. Strong nonresonant absorption by valence electrons of both the metal and the ligands has thus far limited transient absorption spectroscopy to thin-film or gas-phase samples, thus limiting opportunities to study important contributions of solvation.[41] This restriction may soon be lifted by new developments in liquid sheet-jet delivery systems, which provide stable, thickness-tunable platforms for spectroscopy in the hard and soft X-ray spectroscopic regions.[42−45] Such delivery systems have enabled observation of ground-state spectra in the 200−400 eV water window using high-harmonic sources.[44]

Implications for Fe^{II} Photochemistry. The results presented in this work show that the relaxation mechanism of photoexcited $Fe(phen)_3^{2+}$ is similar to that of $Fe(bpy)_3^{2+}$: a metal-centered triplet state is formed that lasts for tens of fs before relaxing to the quintet state, likely by means of non-first-order kinetics. Such fast time scales, which require strong spin−orbit coupling, suggest that the wave function might evolve in a continuous fashion until it localizes in the quintet.[46] In other words, during the first 200 fs, is spin a good quantum number, or is the system better described as a quantum admixture of the MLCT, ^{3}T, and $^5T_{2g}$ states?[47,48] The M-edge XANES results presented here show that the transient spectra are in fact well-described in terms of pure spin states, with no evidence for continuous peak shifts that should be seen if the electronic character evolves gradually.

The present work also highlights the importance of the shape of the excited-state surfaces in directing the ultrafast dynamics. In the case of $Fe(phen)_3^{2+}$, the 39 fs triplet lifetime gives little time for tetragonal distortions, and the subsequent vibration on the quintet surface can be well-described as a single Fe−N symmetric stretch. This finding contrasts with the behavior of the less-symmetric compound $Fe(phen)_2(NCS)_2$ complex studied by Cammarata et al.,[34] in which sequential activation of breathing and bending modes is observed. Kinetic control of relaxation dynamics has been identified as an important design principle, which can be realized through changing the curvature of metal-centered potential energy surfaces by means of ligand modification.[4] Both the mode-specific spectral changes observed here with M-edge XANES and the direct structural information afforded by femtosecond extended X-ray absorption fine structure (EXAFS) and scattering will aid in such design strategies.

One of the enduring puzzles in this field is the observation that, upon direct excitation into the ^{3}T state at low temperature, only 80% of the excited states are trapped in the $^5T_{2g}$ state, with the other 20% relaxing to the $^1A_{1g}$ ground state.[49] This branching ratio appears incompatible with the 100% quantum yield of $^5T_{2g}$ formation after MLCT excitation, a fact that was cited as partial evidence for the direct MLCT → $^5T_{2g}$ pathway.[14] As shown by the present work and the XES results of Kjær et al., the ^{3}T → $^5T_{2g}$ crossing occurs at a highly compressed geometry for both the triplet and the quintet, leading to a large vibrational coupling term between the two states and accelerating spin crossover.[9,50] Direct excitation to the ligand field states imparts significantly less vibrational energy to the system and likely directs the excited states to different seams in the excited-state surface.

Finally, we note the general importance of state-specific spectroscopy when assigning excited-state relaxation pathways. The metastable state of the strong-field complex $Fe(dcpp)_2^{2+}$ was initially proposed to be a metal-centered triplet on the basis of its relatively short excited-state lifetime (270 ps),[51] but subsequent transient XES and EXAFS studies revealed instead a quintet state with high anisotropy in the primary coordination sphere.[52] The clear evidence for metal-centered states provided by core-level spectroscopy will be an important diagnostic tool for designing new earth-abundant chromophores capable of displacing Ru and Ir for phototoredox chemistry and solar energy conversion.

CONCLUSION

In this work, we use M-edge XANES spectroscopy to show that photoexcitation of the MLCT transition of $Fe(phen)_3^{2+}$ forms a metastable $^5T_{2g}$ state via a ^{3}T intermediate. This intermediate state is conclusively identified on the basis of ligand field multiplet simulations of the extracted excited state spectrum. We also observed coherent oscillations consistent with vibrational relaxation on the $^5T_{2g}$ potential energy surface, and the spectrum of this oscillation fingerprints the Fe−N symmetric stretch activated by spin crossover. The rich information in $M_{2,3}$-edge XANES, combined with the increasing accessibility of tabletop sources, makes transient studies in the XUV spectral region a powerful tool for resolving ultrafast photophysics of transition metal complexes.

ASSOCIATED CONTENT

Supporting Information

The Supporting Information is available free of charge on the ACS Publications website at DOI: 10.1021/jacs.9b07332.

Further information about experimental and computational details (PDF)

AUTHOR INFORMATION

Corresponding Author

*vuraweis@illinois.edu

ORCID

Gregory S. Girolami: 0000-0002-7295-1775

Josh Vura-Weis: 0000-0001-7734-3130

Author Contributions

†K.Z. and R.A. contributed equally to this work.

Notes

The authors declare no competing financial interest.

DOI: 10.1021/jacs.9b07332
J. Am. Chem. Soc. 2019, 141, 17180−17188

■ ACKNOWLEDGMENTS

This material is based upon work supported by the National Science Foundation under Grant no. 1555245. The transient XUV instrument, including the nonlinear optical parametric amplifier, was built with funding from the Air Force Office of Scientific Research under AFOSR Award no. FA9550-14-1-0314. G.S.G. acknowledges the support of the William and Janet Lycan Fund at the University of Illinois.

■ REFERENCES

(1) Abrahamsson, M. Solar Energy Conversion Using Iron Polypyridyl Type Photosensitizers - A Viable Route for the Future? *Photochemistry* **2016**, *44*, 285−295.
(2) Prier, C. K.; Rankic, D. A.; MacMillan, D. W. C. Visible Light Photoredox Catalysis with Transition Metal Complexes: Applications in Organic Synthesis. *Chem. Rev.* **2013**, *113* (7), 5322−5363.
(3) Wenger, O. S. Is Iron the New Ruthenium? *Chem. - Eur. J.* **2019**, *25* (24), 6043−6052.
(4) McCusker, J. K. Electronic Structure in the Transition Metal Block and Its Implications for Light Harvesting. *Science* **2019**, *363* (6426), 484−488.
(5) Kalyanasundaram, K. Photophysics, Photochemistry and Solar Energy Conversion with Tris(Bipyridyl)Ruthenium(II) and Its Analogues. *Coord. Chem. Rev.* **1982**, *46*, 159−244.
(6) Bergkamp, M. A.; Chang, C. K.; Netzel, T. L. Quantum Yield Determinations for Subnanosecond-Lived Excited States and Photoproducts: Applications to Inorganic Complexes and Photosynthetic Models. *J. Phys. Chem.* **1983**, *87* (22), 4441−4446.
(7) Juban, E. A.; Smeigh, A. L.; Monat, J. E.; McCusker, J. K. Ultrafast Dynamics of Ligand-Field Excited States. *Coord. Chem. Rev.* **2006**, *250* (13−14), 1783−1791.
(8) Chábera, P.; Kjaer, K. S.; Prakash, O.; Honarfar, A.; Liu, Y.; Fredin, L. A.; Harlang, T. C. B.; Lidin, S.; Uhlig, J.; Sundström, V.; Lomoth, R.; Persson, P.; Wärnmark, K. Fe^{II} Hexa N-Heterocyclic Carbene Complex with a 528 ps Metal-To-Ligand Charge-Transfer Excited-State Lifetime. *J. Phys. Chem. Lett.* **2018**, *9* (3), 459−463.
(9) Sousa, C.; de Graaf, C.; Rudavskyi, A.; Broer, R.; Tatchen, J.; Etinski, M.; Marian, C. M. Ultrafast Deactivation Mechanism of the Excited Singlet in the Light-Induced Spin Crossover of $[Fe(2,2'\text{-Bipyridine})_3]^{2+}$. *Chem. - Eur. J.* **2013**, *19* (51), 17541−17551.
(10) van Veenendaal, M.; Chang, J.; Fedro, A. J. Model of Ultrafast Intersystem Crossing in Photoexcited Transition-Metal Organic Compounds. *Phys. Rev. Lett.* **2010**, *104* (6), 067401.
(11) Lemke, H. T.; Kjær, K. S.; Hartsock, R.; Van Driel, T. B.; Chollet, M.; Glownia, J. M.; Song, S.; Zhu, D.; Pace, E.; Matar, S. F.; Nielsen, M. M.; Benfatto, M.; Gaffney, K. J.; Collet, E.; Cammarata, M. Coherent Structural Trapping through Wave Packet Dispersion during Photoinduced Spin State Switching. *Nat. Commun.* **2017**, *8*, 15342.
(12) Kjær, K. S.; Van Driel, T. B.; Harlang, T. C. B.; Kunnus, K.; Biasin, E.; Ledbetter, K.; Hartsock, R. W.; Reinhard, M. E.; Koroidov, S.; Li, L.; Laursen, M. G.; Hansen, F. B.; Vester, P.; Christensen, M.; Haldrup, K.; Nielsen, M. M.; Dohn, A. O.; Pápai, M. I.; Møller, K. B.; Chabera, P.; Liu, Y.; Tatsuno, H.; Timm, C.; Jarenmark, M.; Uhlig, J.; Sundstöm, V.; Wärnmark, K.; Persson, P.; Németh, Z.; Szemes, D. S.; Bajnóczi, É.; Vankó, G.; Alonso-Mori, R.; Glownia, J. M.; Nelson, S.; Sikorski, M.; Sokaras, D.; Canton, S. E.; Lemke, H. T.; Gaffney, K. J. Finding Intersections between Electronic Excited State Potential Energy Surfaces with Simultaneous Ultrafast X-Ray Scattering and Spectroscopy. *Chem. Sci.* **2019**, *10* (22), 5749−5760.
(13) Zhang, W.; Alonso-Mori, R.; Bergmann, U.; Bressler, C.; Chollet, M.; Galler, A.; Gawelda, W.; Hadt, R. G.; Hartsock, R. W.; Kroll, T.; Kjær, K. S.; Kubiček, K.; Lemke, H. T.; Liang, H. W.; Meyer, D. A.; Nielsen, M. M.; Purser, C.; Robinson, J. S.; Solomon, E. I.; Sun, Z.; Sokaras, D.; van Driel, T. B.; Vankó, G.; Weng, T.-C.; Zhu, D.; Gaffney, K. J. Tracking Excited-State Charge and Spin Dynamics in Iron Coordination Complexes. *Nature* **2014**, *509*, 345−348.
(14) Auböck, G.; Chergui, M. Sub-50-Fs Photoinduced Spin Crossover in $[Fe(Bpy)_3]^{2+}$. *Nat. Chem.* **2015**, *7* (8), 629−633.
(15) Chábera, P.; Fredin, L. A.; Kjær, K. S.; Rosemann, N. W.; Lindh, L.; Prakash, O.; Liu, Y.; Wärnmark, K.; Uhlig, J.; Sundström, V.; Yartsev, A.; Persson, P. Band-Selective Dynamics in Charge-Transfer Excited Iron Carbene Complexes. *Faraday Discuss.* **2019**, *216*, 191−210.
(16) Kjær, K. S.; Kaul, N.; Prakash, O.; Chábera, P.; Rosemann, N. W.; Honarfar, A.; Gordivska, O.; Fredin, L. A.; Bergquist, K.-E.; Häggström, L.; Ericsson, T.; Lindh, L.; Yartsev, A.; Styring, S.; Huang, P.; Uhlig, J.; Bendix, J.; Strand, D.; Sundström, V.; Persson, P.; Lomoth, R.; Wärnmark, K. Luminescence and Reactivity of a Charge-Transfer Excited Iron Complex with Nanosecond Lifetime. *Science* **2019**, *363* (6424), 249−253.
(17) Ryland, E. S.; Lin, M.-F.; Verkamp, M. A.; Zhang, K.; Benke, K.; Carlson, M.; Vura-Weis, J. Tabletop Femtosecond M-Edge X-Ray Absorption Near-Edge Structure of FeTPPCl: Metalloporphyrin Photophysics from the Perspective of the Metal. *J. Am. Chem. Soc.* **2018**, *140* (13), 4691−4696.
(18) Chatterley, A. S.; Lackner, F.; Pemmaraju, C. D.; Neumark, D. M.; Leone, S. R.; Gessner, O. Dissociation Dynamics and Electronic Structures of Highly Excited Ferrocenium Ions Studied by Femtosecond XUV Absorption Spectroscopy. *J. Phys. Chem. A* **2016**, *120* (48), 9509−9518.
(19) Vura-Weis, J.; Jiang, C.-M.; Liu, C.; Gao, H.; Lucas, J. M.; de Groot, F. M. F.; Yang, P.; Alivisatos, A. P.; Leone, S. R. Femtosecond $M_{2,3}$-Edge Spectroscopy of Transition-Metal Oxides: Photoinduced Oxidation State Change in α-Fe_2O_3. *J. Phys. Chem. Lett.* **2013**, *4* (21), 3667−3671.
(20) Zhang, K.; Girolami, G. S.; Vura-Weis, J. Improved Charge Transfer Multiplet Method to Simulate M - and L -Edge X-Ray Absorption Spectra of Metal-Centered Excited States. *J. Synchrotron Radiat.* **2018**, *25* (5), 1600−1608.
(21) Baker, L. R.; Jiang, C.-M.; Kelly, S. T.; Lucas, J. M.; Vura-Weis, J.; Gilles, M. K.; Alivisatos, A. P.; Leone, S. R. Charge Carrier Dynamics of Photoexcited Co_3O_4 in Methanol: Extending High Harmonic Transient Absorption Spectroscopy to Liquid Environments. *Nano Lett.* **2014**, *14* (10), 5883−5890.
(22) Zhang, K.; Lin, M. F.; Ryland, E. S.; Verkamp, M. A.; Benke, K.; De Groot, F. M. F.; Girolami, G. S.; Vura-Weis, J. Shrinking the Synchrotron: Tabletop Extreme Ultraviolet Absorption of Transition-Metal Complexes. *J. Phys. Chem. Lett.* **2016**, *7*, 3383−3387.
(23) Carneiro, L. M.; Cushing, S. K.; Liu, C.; Su, Y.; Yang, P.; Alivisatos, A. P.; Leone, S. R. Excitation-Wavelength-Dependent Small Polaron Trapping of Photoexcited Carriers in α-Fe_2O_3. *Nat. Mater.* **2017**, *16* (8), 819−825.
(24) Cowan, R. D. *The Theory of Atomic Structure and Spectra*; University of California Press: Berkeley, 1981.
(25) de Groot, F.; Kotani, A. *Core Level Spectroscopy of Solids*; CRC Press: 2008.
(26) Warner, B.; Oberg, J. C.; Gill, T. G.; El Hallak, F.; Hirjibehedin, C. F.; Serri, M.; Heutz, S.; Arrio, M.-A.; Sainctavit, P.; Mannini, M.; Poneti, G.; Sessoli, R.; Rosa, P. Temperature- and Light-Induced Spin Crossover Observed by X-Ray Spectroscopy on Isolated Fe(II) Complexes on Gold. *J. Phys. Chem. Lett.* **2013**, *4* (9), 1546−1552.
(27) Huse, N.; Cho, H.; Hong, K.; Jamula, L.; de Groot, F. M. F.; Kim, T. K.; McCusker, J. K.; Schoenlein, R. W. Femtosecond Soft X-Ray Spectroscopy of Solvated Transition-Metal Complexes: Deciphering the Interplay of Electronic and Structural Dynamics. *J. Phys. Chem. Lett.* **2011**, *2* (8), 880−884.
(28) Gawelda, W.; Cannizzo, A.; Pham, V. T.; Van Mourik, F.; Bressler, C.; Chergui, M. Ultrafast Nonadiabatic Dynamics of $[Fe^{II}(Bpy)_3]^{2+}$ in Solution. *J. Am. Chem. Soc.* **2007**, *129* (26), 8199−8206.
(29) Nitzan, A. *Chemical Dynamics in Condensed Phases*; Oxford University Press: New York, 2006.
(30) Consani, C.; Prémont-Schwarz, M.; Elnahhas, A.; Bressler, C.; Van Mourik, F.; Cannizzo, A.; Chergui, M. Vibrational Coherences

DOI: 10.1021/jacs.9b07332
J. Am. Chem. Soc. 2019, 141, 17180−17188

and Relaxation in the High-Spin State of Aqueous $[Fe^{II}(Bpy)_3]^{2+}$. *Angew. Chem., Int. Ed.* **2009**, *48* (39), 7184−7187.
(31) Monat, J. E.; McCusker, J. K. Femtosecond Excited-State Dynamics of an Iron(II) Polypyridyl Solar Cell Sensitizer Model. *J. Am. Chem. Soc.* **2000**, *122* (17), 4092−4097.
(32) Lemke, H. T.; Kjær, K. S.; Hartsock, R.; van Driel, T. B.; Chollet, M.; Glownia, J. M.; Song, S.; Zhu, D.; Pace, E.; Matar, S. F.; Nielsen, M. M.; Benfatto, M.; Gaffney, K. J.; Collet, E.; Cammarata, M. Coherent Structural Trapping through Wave Packet Dispersion during Photoinduced Spin State Switching. *Nat. Commun.* **2017**, *8*, 15342.
(33) Ronayne, K. L.; Paulsen, H.; Höfer, A.; Dennis, A. C.; Wolny, J. A.; Chumakov, A. I.; Schünemann, V.; Winkler, H.; Spiering, H.; Bousseksou, A.; Gütlich, P.; Trautwein, A. X.; McGarvey, J. J. Vibrational Spectrum of the Spin Crossover Complex $[Fe(Phen)_2(NCS)_2]$ Studied by IR and Raman Spectroscopy, Nuclear Inelastic Scattering and DFT Calculations. *Phys. Chem. Chem. Phys.* **2006**, *8* (40), 4685−4693.
(34) Cammarata, M.; Bertoni, R.; Lorenc, M.; Cailleau, H.; Di Matteo, S.; Mauriac, C.; Matar, S. F.; Lemke, H.; Chollet, M.; Ravy, S.; Laulhé, C.; Létard, J.-F.; Collet, E. Sequential Activation of Molecular Breathing and Bending during Spin-Crossover Photoswitching Revealed by Femtosecond Optical and X-Ray Absorption Spectroscopy. *Phys. Rev. Lett.* **2014**, *113* (22), 227402.
(35) Miller, N. A.; Deb, A.; Alonso-Mori, R.; Glownia, J. M.; Kiefer, L. M.; Konar, A.; Michocki, L. B.; Sikorski, M.; Sofferman, D. L.; Song, S.; Toda, M. J.; Wiley, T. E.; Zhu, D.; Kozlowski, P. M.; Kubarych, K. J.; Penner-Hahn, J. E.; Sension, R. J. Ultrafast X-Ray Absorption Near Edge Structure Reveals Ballistic Excited State Structural Dynamics. *J. Phys. Chem. A* **2018**, *122* (22), 4963−4971.
(36) Peng, G.; deGroot, F. M. F.; Haemaelaeinen, K.; Moore, J. A.; Wang, X.; Grush, M. M.; Hastings, J. B.; Siddons, D. P.; Armstrong, W. H. High-Resolution Manganese x-Ray Fluorescence Spectroscopy. Oxidation-State and Spin-State Sensitivity. *J. Am. Chem. Soc.* **1994**, *116* (7), 2914−2920.
(37) Pollock, C. J.; Delgado-Jaime, M. U.; Atanasov, M.; Neese, F.; DeBeer, S. Kβ Mainline X-Ray Emission Spectroscopy as an Experimental Probe of Metal-Ligand Covalency. *J. Am. Chem. Soc.* **2014**, *136* (26), 9453−9463.
(38) Lee, N.; Petrenko, T.; Bergmann, U.; Neese, F.; DeBeer, S. Probing Valence Orbital Composition with Iron Kβ X-Ray Emission Spectroscopy. *J. Am. Chem. Soc.* **2010**, *132* (28), 9715−9727.
(39) Nass Kovacs, G.; Colletier, J.-P.; Grünbein, M. L.; Yang, Y.; Stensitzki, T.; Batyuk, A.; Carbajo, S.; Doak, R. B.; Ehrenberg, D.; Foucar, L.; Gasper, R.; Gorel, A.; Hilpert, M.; Kloos, M.; Koglin, J. E.; Reinstein, J.; Roome, C. M.; Schlesinger, R.; Seaberg, M.; Shoeman, R. L.; Stricker, M.; Boutet, S.; Haacke, S.; Heberle, J.; Heyne, K.; Domratcheva, T.; Barends, T. R. M.; Schlichting, I. Three-Dimensional View of Ultrafast Dynamics in Photoexcited Bacteriorhodopsin. *Nat. Commun.* **2019**, *10*, 3177.
(40) Schmidt, B.; Sobotta, C.; Heinz, B.; Laimgruber, S.; Braun, M.; Gilch, P. Excited-State Dynamics of Bacteriorhodopsin Probed by Broadband Femtosecond Fluorescence Spectroscopy. *Biochim. Biophys. Acta, Bioenerg.* **2005**, *1706* (1−2), 165−173.
(41) Kjær, K. S.; Kunnus, K.; Harlang, T. C. B.; Van Driel, T. B.; Ledbetter, K.; Hartsock, R. W.; Reinhard, M. E.; Koroidov, S.; Li, L.; Laursen, M. G.; Biasin, E.; Hansen, F. B.; Vester, P.; Christensen, M.; Haldrup, K.; Nielsen, M. M.; Chábera, P.; Liu, Y.; Tatsuno, H.; Timm, C.; Uhlig, J.; Sundstöm, V.; Németh, Z.; Szemes, D. S.; Bajnóczi, É.; Vankó, G.; Alonso-Mori, R.; Glownia, J. M.; Nelson, S.; Sikorski, M.; Sokaras, D.; Lemke, H. T.; Canton, S. E.; Wärnmark, K.; Persson, P.; Cordones, A. A.; Gaffney, K. J. Solvent Control of Charge Transfer Excited State Relaxation Pathways in $[Fe(2,2'\text{-Bipyridine})(CN)_4]^{2-}$. *Phys. Chem. Chem. Phys.* **2018**, *20* (6), 4238−4249.
(42) Koralek, J. D.; Kim, J. B.; Brůža, P.; Curry, C. B.; Chen, Z.; Bechtel, H. A.; Cordones, A. A.; Sperling, P.; Toleikis, S.; Kern, J. F.; Moeller, S. P.; Glenzer, S. H.; DePonte, D. P. Generation and Characterization of Ultrathin Free-Flowing Liquid Sheets. *Nat. Commun.* **2018**, *9* (1), 1353.
(43) Ekimova, M.; Quevedo, W.; Faubel, M.; Wernet, P.; Nibbering, E. T. J. A Liquid Flatjet System for Solution Phase Soft-x-Ray Spectroscopy. *Struct. Dyn.* **2015**, *2* (5), 054301.
(44) Kleine, C.; Ekimova, M.; Goldsztejn, G.; Raabe, S.; Strüber, C.; Ludwig, J.; Yarlagadda, S.; Eisebitt, S.; Vrakking, M. J. J.; Elsaesser, T.; Nibbering, E. T. J.; Rouzée, A. Soft X-Ray Absorption Spectroscopy of Aqueous Solutions Using a Table-Top Femtosecond Soft X-Ray Source. *J. Phys. Chem. Lett.* **2019**, *10* (1), 52−58.
(45) Kubin, M.; Guo, M.; Ekimova, M.; Baker, M. L.; Kroll, T.; Källman, E.; Kern, J.; Yachandra, V. K.; Yano, J.; Nibbering, E. T. J.; Lundberg, M.; Wernet, P. Direct Determination of Absolute Absorption Cross Sections at the L-Edge of Dilute Mn Complexes in Solution Using a Transmission Flatjet. *Inorg. Chem.* **2018**, *57* (9), 5449−5462.
(46) Brady, C.; McGarvey, J. J.; McCusker, J. K.; Toftlund, H.; Hendrickson, D. N. Time-Resolved Relaxation Studies of Spin Crossover Systems in Solution. In *Spin Crossover in Transition Metal Compounds III*; Springer-Verlag: Berlin/Heidelberg, 2006; pp 1−22.
(47) Maltempo, M. M.; Moss, T. H. The Spin 3/2 State and Quantum Spin Mixtures in Haem Proteins. *Q. Rev. Biophys.* **1976**, *9* (2), 181−215.
(48) Maltempo, M. M. Magnetic State of an Unusual Bacterial Heme Protein. *J. Chem. Phys.* **1974**, *61* (7), 2540−2547.
(49) Hauser, A. Intersystem Crossing in the $[Fe(Ptz)_6](BF_4)_2$ Spin Crossover System (Ptz = 1-propyltetrazole). *J. Chem. Phys.* **1991**, *94* (4), 2741−2748.
(50) Penfold, T. J.; Gindensperger, E.; Daniel, C.; Marian, C. M. Spin-Vibronic Mechanism for Intersystem Crossing. *Chem. Rev.* **2018**, *118* (15), 6975−7025.
(51) Jamula, L. L.; Brown, A. M.; Guo, D.; McCusker, J. K. Synthesis and Characterization of a High-Symmetry Ferrous Polypyridyl Complex: Approaching the 5T2/3T1 Crossing Point for FeII. *Inorg. Chem.* **2014**, *53* (1), 15−17.
(52) Britz, A.; Gawelda, W.; Assefa, T. A.; Jamula, L. L.; Yarranton, J. T.; Galler, A.; Khakhulin, D.; et al. Using Ultrafast X-Ray Spectroscopy To Address Questions in Ligand-Field Theory: The Excited State Spin and Structure of $[Fe(Dcpp)_2]^{2+}$. *Inorg. Chem.* **2019**, *58* (14), 9341−9350.

DOI: 10.1021/jacs.9b07332
J. Am. Chem. Soc. 2019, 141, 17180−17188